SLUG FLOW PREDICTION WITH THE VOLUME OF FLUID MODEL

M. Febres, mijail_febres@hotmail.com
A.O. Nieckele, nieckele@puc-rio.br
Department of Mechanical Engineering, PUC-Rio, Rio de Janeiro, RJ, 22453-900, BRAZIL

Abstract. *Numerical simulation of a single unit slug was performed with the VOF model. The slug translation velocity was obtained and the coefficients of the Bendiksen equation were adjusted to fit all cases. The computed velocity was compared with the experimental data obtained with PIV and Laser Doppler anemometer. It can be said that a very good agreement was obtained.*

Keywords*: slug flow, horizontal pipeline, VOF, three-dimensional*

1. INTRODUCTION

Multiphase flow is very common in the petroleum industry and depending on the phase's superficial velocities during its transport, different flow patterns can be found, such as "smooth stratified", "wavy stratified", "elongated bubble", "slug", "annular", "chaotic", "bubble", etc. One of the most common flow patterns during operation in petroleum processing facilities is the "slug" pattern. There have been many attempts in the literature to model a two-phase slug flow. One of the first models, presented by Wallis (1969), is based on the concept of the single unit slug with a reference frame moving with the tip of the bubble. Later, Taitel and Barnea (1990) using the same concept, divided the single unit slug into two parts: the liquid slug and liquid film zones. Fagundes Netto et al. (1999) developed a model based on mass and momentum conservation equations to predict the shape of the tip and tail of the gas bubble, as well as the liquid slug, and presented a comparison with experimental data. Taitel et al. (2000) showed that a negative pipe inclination damps slug formation. Orell et al. (2004) used a sub-model of Taitel and Barnea (1990) model, and obtained an increase of the pressure loss, obtaining good results in agreement with experimental data. De Freitas et al. (2008) applied the single unit slug concept through a vertical pipe and studied the effect of gas expansion. Several codes have been developed and are widely used, such as PLAC (Black et al., 1990) and OLGA (Bendiksen et al., 1991).

Bendiksen (1984), Cook and Behnia (2000) and Bertola (2002) among others have investigated experimentally slug flows, focusing on global measurements such as pressure drop, overall void fraction and statistical parameters such as slug length distribution, slug frequency and film thickness. Probably due to the complex nature of the slug flow pattern, relatively few papers were found reporting results on detailed measurements of the flow field in the liquid slug and film layer under the gas bubble. Detailed information on the flow behavior is critical to the proper understanding of the physical mechanisms governing the flow.

Numerical simulation has became a very important tool to predict multiphase flow inside pipelines due to the worldwide increasing fuel demand for industry, as well as higher standard requirements for equipment design for petroleum processing and transport. For an efficient equipment or pipe design, it is desired to determine the individual hydrodynamic characteristics of each flow pattern, such as pressure drop and flow intermittence parameters.

In the present work, the commercial CFD software FLUENT™ was employed to solve numerically the air/water two-phase slug flow with the single unit slug approach. The results such as bubble shape and film velocity profiles were compared with measured data presenting good agreement.

2. MATHEMATICAL MODEL

To determine the two-phase slug flow field inside a horizontal pipeline, the VOF (volume of fluid) model (Hirt and Nichols, 1981) was selected. The VOF model is based on the solution of one single set of conservation equations of mass and momentum. An auxiliary variable, named "volume fraction" α_i, is considered to identify the region occupied by each phase, it is equal 1 in one phase and zero in the other one. The sum of volume fractions is equal to 1, i.e.,

$$\alpha_g + \alpha_\ell = 1. \tag{1}$$

.

All variables and properties fields are shared by both phases, and they represent average values. Density and viscosity are obtained as follows:

$$\rho = \alpha_g \rho_g + \alpha_\ell \rho_\ell \tag{2}$$

$$\mu = \alpha_g \mu_g + \alpha_\ell \mu_\ell \tag{3}$$

The interface tracking is determined by assuming a material derivative of the interface equal to zero for a referential on the interface, thus

$$\frac{\partial \alpha_g}{\partial t} + \vec{u} \bullet \nabla \alpha_g = 0 \tag{4}$$

where $\vec{u}$ is the time average velocity vector.

The Reynolds average continuity and momentum conservation equations can be written as

$$\frac{\partial}{\partial t}(\rho \vec{u}) + \nabla \bullet (\rho \vec{u}) = 0 \tag{5}$$

$$\frac{\partial}{\partial t}(\rho \vec{u}) + \nabla \bullet (\rho \vec{u}\,\vec{u}) = -\nabla p + \rho \vec{g} + \nabla \bullet [\mu_{ef}\ 2\,\underline{\underline{S}}] + \rho \vec{g} + \vec{F} \quad ; \quad \underline{\underline{S}} = \frac{1}{2}(\nabla \vec{u} + \nabla \vec{u}^T) \tag{6}$$

where p is the pressure, $\vec{g}$ is the gravity acceleration vector, $\mu_{ef} = \mu + \mu_t$ is the effective viscosity, μ_t is the turbulent viscosity, $\underline{\underline{S}}$ is the mean rate of strain tensor and $\vec{F}$ is an external force which takes in account the effects of surface tension ($\sigma_{g\ell}$) of two phases.

The external force term based on the CSF model (Continuum Surface Force) developed by Brackbill et al. (1992) based on the interface curvature $\Re$ is added to the momentum equation to account the effects of surface tension of two phases.

$$\vec{F} = \sigma_{g\ell} \frac{\rho\, \Re\, \nabla \alpha_g}{(\rho_g + \rho_\ell)/2} \quad ; \quad \Re = \nabla \bullet \hat{n} \quad ; \quad \hat{n} = \frac{\vec{n}}{|\vec{n}|} \quad ; \quad \vec{n} = \nabla \alpha_g \tag{7}$$

The turbulence was modeled with the κ–ε RNG model (Yakhot et al., 1992). For high Reynolds number, the turbulent viscosity is

$$\mu_t = C_\mu\, \rho\, \kappa^2 / \varepsilon \quad ; \quad C_\mu = 0.0845 \tag{8}$$

where κ is the turbulent kinetic energy and ε its dissipation rate, and are obtained from the following transport equations:

$$\frac{\partial}{\partial t}(\rho \kappa) + \nabla \bullet (\rho \vec{u}\, \kappa) = \nabla \bullet [\lambda_\kappa\ \mu_{ef} \nabla \kappa] + G_\kappa - \rho\, \varepsilon \quad ; \quad G_\kappa = \mu_t\, S^2 \quad ; \quad S = \sqrt{2\, S_{ij}\, S_{ij}} \tag{9}$$

$$\frac{\partial}{\partial t}(\rho \varepsilon) + \nabla \bullet (\rho \vec{u}\, \varepsilon) = \nabla \bullet [\lambda_\varepsilon\ \mu_{ef}\ \nabla \varepsilon] + C_{1\varepsilon} \frac{\varepsilon}{\kappa} G_\kappa - C_{2\varepsilon}^* \rho \frac{\varepsilon^2}{\kappa} \quad ; \quad C_{2\varepsilon}^* = C_{2\varepsilon} + \frac{C_\mu\, \eta^3 (1 - \eta/\eta_0)}{1 + \beta\, \eta^3} \tag{10}$$

In these equations, G_κ represents the generation of turbulence kinetic energy due to the mean velocity gradients. The destruction of ε depends on $\eta = S\, \kappa/\varepsilon$. The empirical constants are: $C_{1\varepsilon} = 1.42$, $C_{2\varepsilon} = 1.68$, $\lambda_o = 1$, $\beta = 0.012$ and $\eta_0 = 4.38$. λ_k and λ_ε are the inverse Prandtl numbers for κ and ε respectively, obtained from the following expressions:

$$\left|\frac{\lambda_{\kappa,\varepsilon} - 1.3929}{\lambda_o - 1.3929}\right|^{0.6321} \left|\frac{\lambda_{\kappa,\varepsilon} + 2.3929}{\lambda_o + 2.3929}\right|^{0.3679} = \frac{\mu}{\mu_{ef}} \tag{11}$$

To predict a single unit cell, a reference frame moving with the bubble was employed. Therefore, at the pipe wall a slug translational velocity was prescribed. At the entrance of the domain, the mixture velocity was imposed as $W_m = w_{s\ell} + w_{sg}$, where $w_{s\ell}$ and w_{sg} are the liquid and gas superficial velocities, relative to the wall. The entrance turbulent quantities were

$$\kappa = (3/2)\,(W_m\, \zeta)^2 \text{ and } \varepsilon = C_\mu^{3/4}\, \kappa^{3/2} / \ell_c, \tag{12}$$

with ζ=0.05 and ℓ_c =0.07 D. At the exit a constant pressure was prescribed.

3. NUMERICAL MODEL

To solve the mathematical model, the commercial software FLUENT™ was employed. It is based on the Finite Volume technique which consists on dividing the computational domain on small control volumes and integrating spatially and temporarily the transport equations over them. First order implicit technique was used for the time integration, while the spatial integration was handled with the second order "QUICK" scheme (Leonard, 1979).

The pressure-velocity coupling was solved with the PISO algorithm (Issa, 1986) and PRESTO was selected as the interpolation scheme for pressure. To reconstruct the interface of the VOF methodology, the "Geometric Reconstruction" technique was applied. The resulting discretization algebraic equations were solved using the AMG (*Algebraic Multigrid Solver)* option (Hutchinson et al., 1986).

The mesh of the circular pipe was generated with GAMBIT™. Solution was obtained with 5100, 29000 and 232.000 control volumes in the cross section, and the intermediate mesh illustrated in Fig. 1a was selected, since the difference in the velocity profile was inferior a 0.5%. Similar test was performed for the axial position and 100 control volumes were selected with the mesh concentrated in the region indicated in the Fig. 1c, with length equal to 2D. At this region, where the tip of the bubble was located, the mesh was approximated uniform in the axial direction (Fig. 1b).

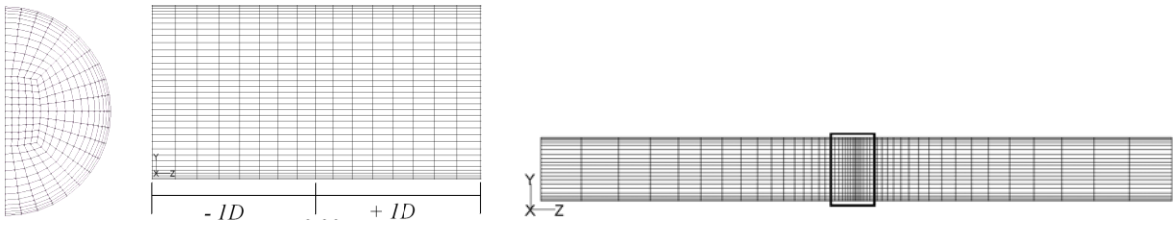

(a) cross section (b) detail at bubble tip. (c) transversal section

Figure 1. Mesh distribution.

The initial condition was defined according to Ujang et al. (2008), in which water volume fraction was set as "1" at first half of the pipe and equal to "0" at the second half (Fig.2a). The wall velocity was initialized according to Bendiksen (1984) models to estimate the slug translational velocity

$$W_T = C_o\, W_m + W_{drift} \quad ; \quad W_{drift} = C_1\sqrt{g\, D} \qquad \begin{matrix} C_o = 1.05 \Rightarrow Fr_c < 3.5 \\ C_o = 1.20 \Rightarrow Fr_c \geq 3.5 \end{matrix} \; ; Fr_c = \frac{w_{sl}}{\sqrt{g\, D}} ; \; C_1 = 0.54 \qquad (13)$$

where C_o stands for the distribution parameter of distribution, g is the gravity acceleration, D the pipe diameter and Fr_c stands for the critic Froude number. The wall velocity obtained with the correlation given by Eq. (10) was a good estimated, but it was corrected based on the flow field, so that the bubble position was maintained fixed inside the computational domain. Usually three iterations were necessary to find a still bubble. Figure 2b illustrates the bubble position inside the domain at different time instants, when imposing the wall velocity in accordance with Eq. (10) while Fig. 2c illustrates the bubble position after the converged wall velocity (translation bubble velocity) was obtained.

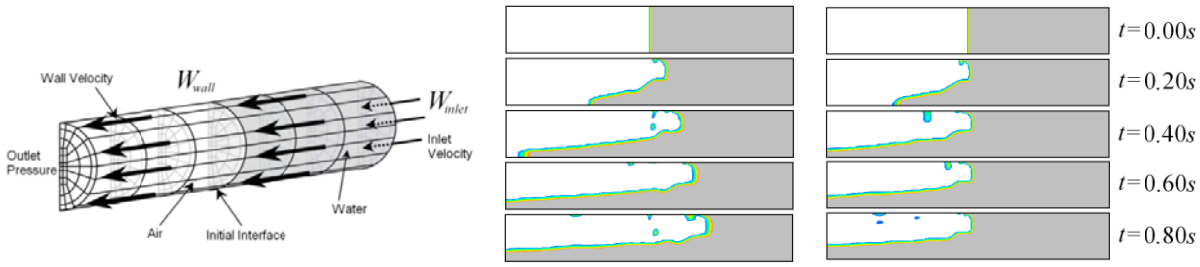

(a) Boundary conditions and domain initialization. (b) Wall velocity (Bendiksen) (c) Converged wall velocity

Figure 2. Boundary conditions, domain initialization and time evolution of Taylor bubble.

4. RESULTS

To verify the ability of the VOF model to predict the slug characteristics, simulations were performed based on two different experiments employing air and water from Fagundes Netto et al (1999)and Fonseca Jr. (2009).

Figures 3 and 4 illustrate the bubble tail and tip shape predicted numerically and the experimental data of Fagundes Netto et al (1999), in pipe with of 0.053 m diameter. Figure 3 corresponds to a mixture velocity of 1.8 m/s and Froude number equal to 2.4, while in Fig. 4, the mixture velocity is equal to 0.6 m/s and Froude number is equal to 0.8. Very similar qualitative results were obtained for both cases. For higher velocities, the water axial penetration (water displacement of the bubble tip away from the wall) at the upper part of the pipe can be clearly seen in Fig. 3, while for the smaller mixture velocity (Fig. 4) the liquid does not wet the pipe wall at the nose region. It can also be seen in the experimental data (Fig. 3) that there is bubble transfer from the tail to the liquid slug; however, this transfer is not predicted numerically. On the other hand, the mixture region is reasonably predicted. Note a smaller liquid film transition to a liquid slug in Fig. 3 than in Fig. 4 due to the higher mixture velocity.

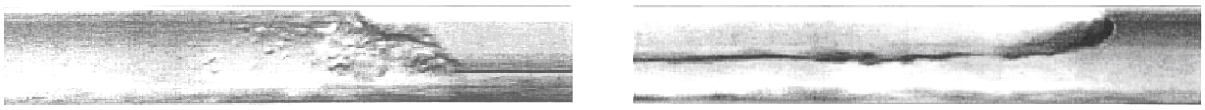

(a) Experimental. Fagundes Neto et al, (1999)

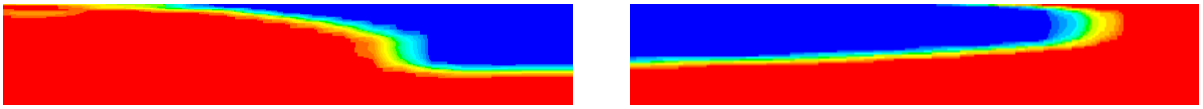

(b) Numerical

Figure 3. Tail and bubble tip shape. W_m = 1.8 m/s, Fr_c = 2.4.

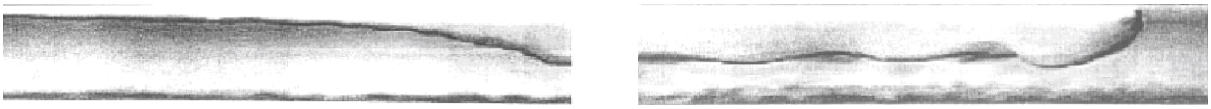

(a) Experimental. Fagundes Neto et al, (1999)

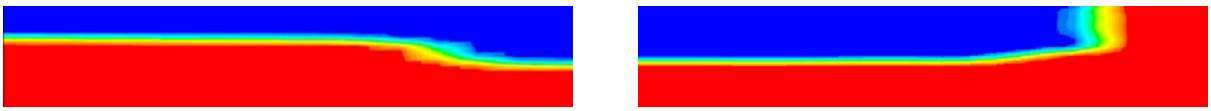

(b) Numerical

Figure 4. Tail and bubble tip shape. W_m = 0.6 m/s, Fr_c= 0.8.

Fonseca Jr. (2009) employed a pipe with diameter D= 0.024 m and L=25 D. Four combinations of gas and liquid superficial velocities were examined. Table 1 presents the superficial velocity of each phase, the resulting mixture velocity, and the superficial velocities ratio. The initial slug translational velocity (Eq. 10) and the converged wall velocity were also included in Table 1. The slug translation velocity and the converged wall velocity presented a variation from 5% to 11%. Therefore, a linear regression of the numerical data for the converged slug translation velocity was performed and the coefficients C_o and C_1 of Eq. (10) were re-evaluated. The corrected coefficients based on the numerical solution were: C_o =1.116 and C_1=0.202 (W_{drift}=0.098 m/s). These values are within the range observed experimentally by Bendiksen (1984) for a pipe with 0.0242 m diameter ($1.009 \leq C_0 \leq 1.188$ and $-0.004\text{m/s} \leq W_{drift} \leq 0.181\text{m/s}$), indicating that the present VOF solution was capable of predicting drift velocity of a slug two phase flow.

Table 1: Test cases.

Cases	w_{sg} (m/s)	w_{sl} (m/s)	W_m (m/s)	w_{sg}/w_{sl}	W_T	W_{wall} (m/s)
1	0.475	0.295	0.770	1.610	1.071	0.956
2	0.475	0.393	0.868	1.209	1.174	1.067
3	0.475	0.516	0.991	0.921	1.303	1.205
4	0.788	0.516	1.304	1.527	1.631	1.552

The bubble nose shape can be evaluated through the axial z_p and radial y_p penetration of the bubble in the liquid slug, measured as indicated in Fig. 5. These quantities are presented in Fig. 6 as a function of the mixture velocity. Note an increase in the radial penetration with an increase of the mixture velocity, as observed experimentally by (Bendiksen, 1984, Rosa et al., 2004). It can also be seen an inclining of the bubble nose in the direction of pipeline center with an increase of the mixture velocity. The variation of y_p with the mixture velocity is small, although small W_m was analyzed.

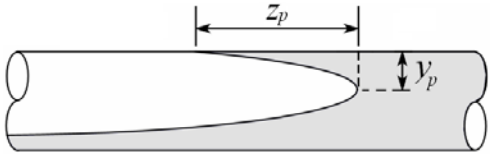

Figure 5. Axial and radial penetration of an elongated bubble.

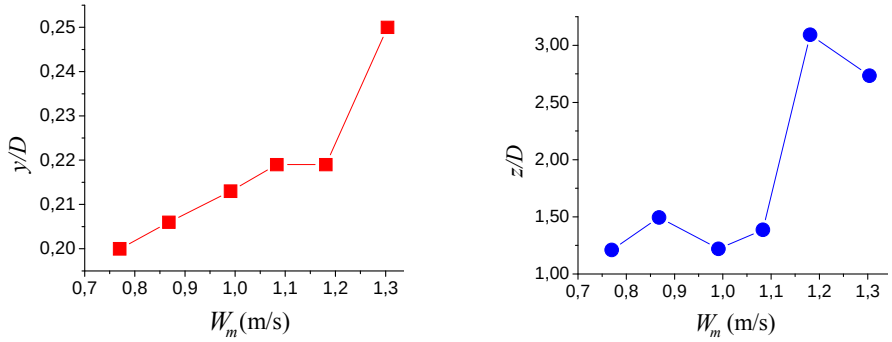

a) Radial penetration b) Axial penetration

Figure 6. Radial and axial penetration.

Figure 7 presents a comparison of present results and the measured velocity profile with the PIV technique (Fonseca Jr, 2009) corresponding to Case 1 and 4. A similar configuration is obtained, where it can be seen that the bubble nose is oriented downward, agreeing with previous experimental observation of Bendiksen (1984). However, the numerical inclination is quite small. Further, the numerical simulation predicted a more round nose than observed experimentally. It can also be seen in the experimental data an increment in the axial and radial penetration with the increase of the mixture velocity, however, this behavior was not observed numerically.

W_m = 1.3 m/s, Fr_c= 1.06. W_m = 0.77 m/s, Fr_c= 0.6.

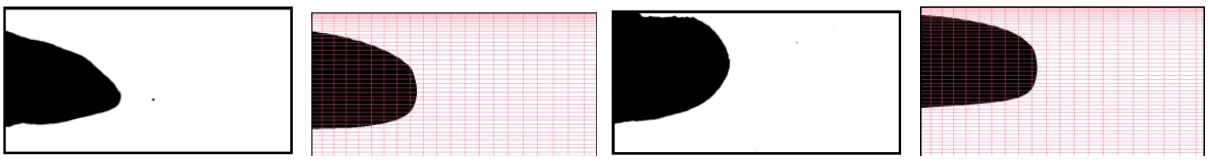

(a) Experimental. Fonseca Jr. (2009). (b) Numerical. (c) Experimental. Fonseca Jr. (2009). (b) Numerical

Figure 7. Bubble tip shape.

To visualize the bubble shape, it is shown in Fig. 8, contours of the volume fraction at five cross section for Case 1. The bubble presents an oval cross section, which gets flatter along the bubble length. Note that the bubble is squeezed and pushed to the upper part of the pipeline. It can be also be seen that at z = - 0.8 D, the bubble touches the wall and the liquid film above it disappears.

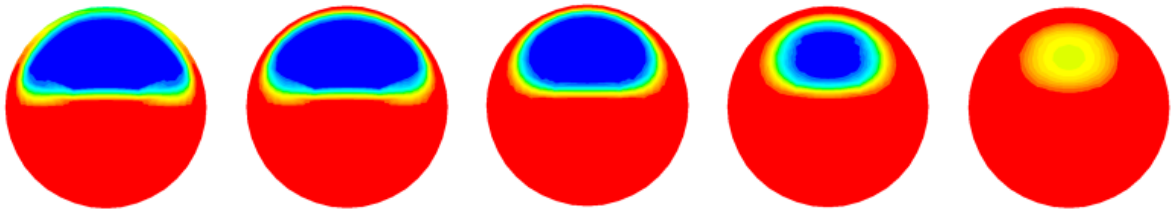

z= – 0.8 D z= – 0.6 D z= – 0.4 D z= – 0.2 D z= 0.0 D

Figure 8. Volume fraction contours at different cross section. Case 1

Axial velocity profiles were obtained along nine vertical lines located at coordinates from -0.8*D* to 0.8*D* relative to tip of the bubble (0.0*D*), as shown in Fig. 9. The coordinates with negative signal will be called from now on "upstream" and coordinates with positive signal will be called "downstream".

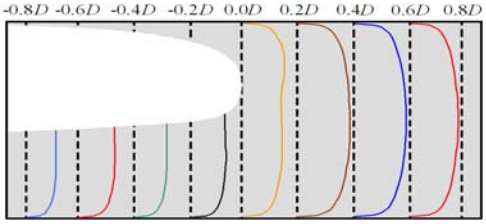

Figure 9. Data Acquisition positions

Detailed results of selected cases are presented here. Figures 10 through 12 show the velocity profiles upstream of the bubble nose, corresponding to the selected Cases 2, 3 and 4, respectively. Experimental data is presented with symbols while numerical results are plotted with continuous lines.

Analyzing Figs. 10-12, it can be seen that there is no experimental data in the gaseous phase, because tracing particles were introduce only in the liquid phase. Due to the smaller viscosity, the gas velocity presents a smaller inclination at the wall, leading to much higher velocities than the liquid phase. An excellent agreement between numerical and experimental data was obtained in the liquid region. However, it can be observed a local reduction on the experimental liquid velocity profile near to the interface. This behavior was not predicted numerically, where a smooth transition from the liquid velocity to the gaseous velocity profile is was obtained. It can also be seen that the maximum gas velocity increases as one moves upstream, while the maximum liquid velocity diminishes, agreeing with the experimental data.

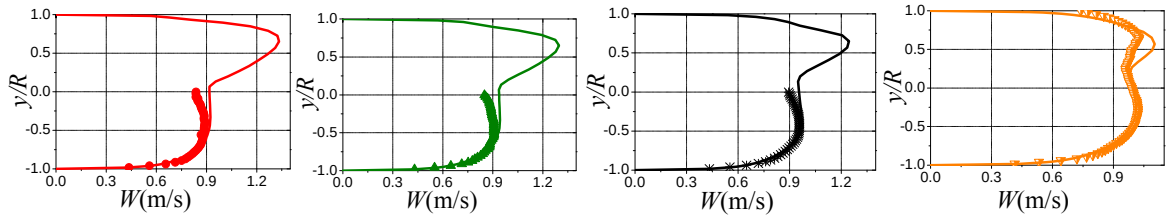

(a) $z = -0.6\ D$ (b) $z = -0.4\ D$ (c) $z = -0.2\ D$ (d) $z = 0.0\ D$

Figure 10: Axial velocity profile, upstream bubble nose. Case 2

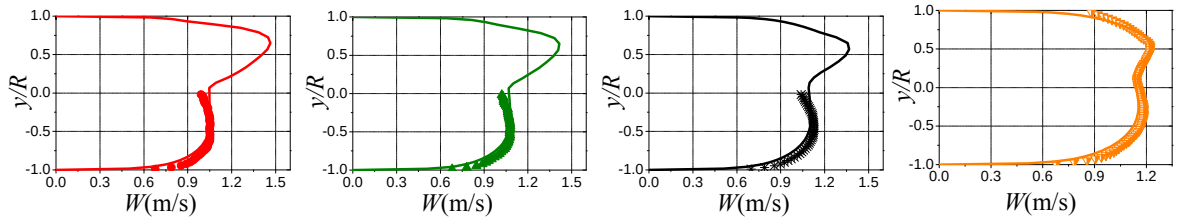

(a) $z = -0.6\ D$ (b) $z = -0.4\ D$ (c) $z = -0.2\ D$ (d) $z = 0.0\ D$

Figure 11. Axial velocity profile, upstream bubble nose. Case 3

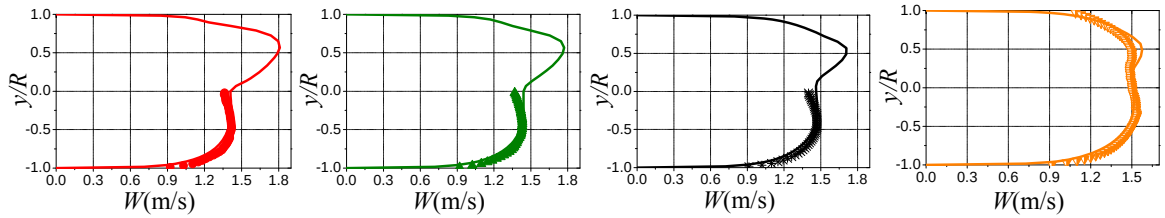

(a) $z = -0.6\ D$ (b) $z = -0.4\ D$ (c) $z = -0.2\ D$ (d) $z = 0.0\ D$

Figure 12. Axial velocity profile, upstream bubble nose. Case 4

Figure 13 presents the velocity profile at the downstream positions for two selected cases (Case 1 and Case 4). The agreement of the numerical results downstream of the Taylor bubble is excellent. According to several researches like Taitel and Barnea (1990), Polonsky et al (1999) and Shemer (2003), velocity profiles in the liquid slug ahead of the bubble must be fully developed. For all cases tested, this behavior was observed.

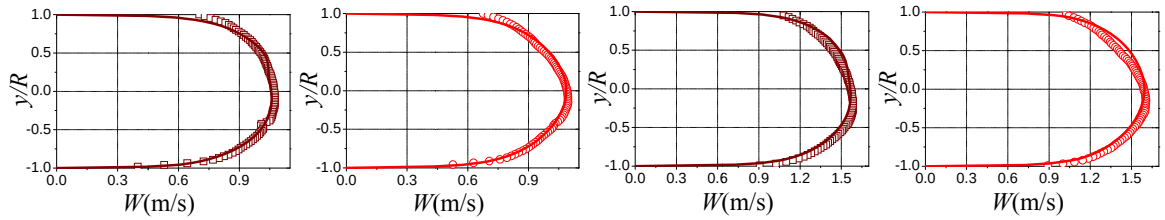

(a) Case 2: $z = +0.2\,D$ (b) Case 2: $z = +0.6\,D$ (c) Case 4: $z = +0.2\,D$ (d) Case 4: $z = +0.6\,D$

Figure 13. Axial velocity profile, downstream bubble nose.

An interesting result to analyze is the velocity field at the pipe cross-section, in the liquid and gas region. Figure 14 illustrates the cross-section velocity vector distribution for Case 1. It can be seen a strong recirculation in the gaseous phase that begins on the interface, climbs to the top of the pipe and returns on the sides. This recirculation is probably responsible for the increase in the bubble diameter as one move upstream of the bubble tip, as shown in Fig. 7.

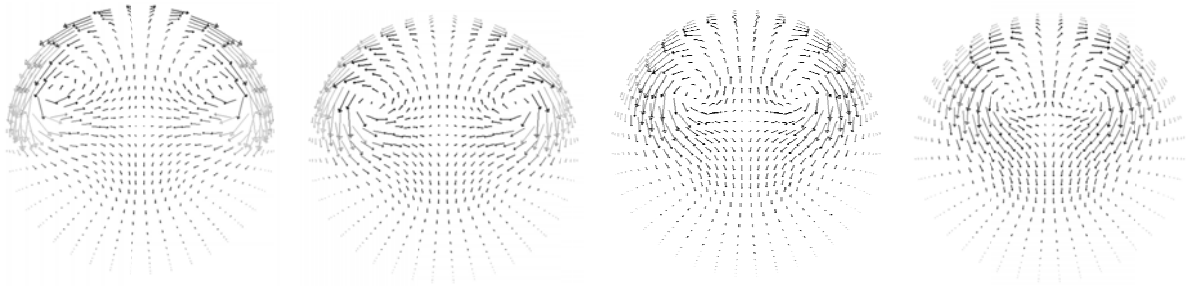

(a) $z = -0.8\,D$ (b) $z = -0.6\,D$ (c) $z = -0.4\,D$ (d) $z = -0.2\,D$

Figure 14. Velocity field at the cross-section, upstream of bubble nose.

5. CONCLUDING REMARKS

Numerical simulation of a single unit slug was performed with the VOF model. The slug translation velocity was obtained and the coefficients of the Bendiksen equation were adjusted to fit all cases. The computed velocity was compared with the experimental data obtained with PIV and Laser Doppler anemometer. It can be said that a very good agreement was obtained.

6. ACKNOWLEDGEMENTS

The authors thank the Brazilian Research Council, CNPq, for the support awarded to this work.

7. REFERENCES

Bendiksen, K. H., 1984, “An Experimental Investigation o f the Motion of long bubbles in inclined pipes”. International Journal of Multiphase Flow, Vol. 10(4), pp. 467-483.

Bendiksen, K.H.; Malnes, D.; Moe, R.; Nuland, S., 1991, “The dynamic two–fluid model OLGA: Theory and Application”. SPE Prod. Eng., Vol. 6, pp. 171–180.

Bertola, V., 2002, “Slug velocity profiles in horizontal gas–liquid flow”. Experiments in Fluids, Vol. 32, pp. 722-727.

Black, P. S., Daniels, L. C., Hoyle, N. C., Jepson , W. P., 1990, “Studying Transient Multi-Phase Flow Using the Pipeline Analysis Code (PLAC)”, Journal Energy Resource Technol., Vol. 112(1), pp. 25.

Brackbill, J.U., Kothe, D.B., Zemach, C., 1992, A continuum method for modeling surface tension”. Journal of Computational Physics, Vol. 100(2), pp. 335-354.

Cook, M. and Behnia, M., 2000, "Slug length prediction in near horizontal gas-liquid intermittent flow". Chemical Engineering Science, Vol. 55, p. 2009–2018.

De Freitas, G.C., Rodrigues, H.T., Morales, E.E.M., Rosa, E. S., Mazza, R. A., 2008, "Algebraic Model for Slug Tracking in Vertical Gas-Liquid Slug Flow". 12th Brazilian Congress of Thermal Engineering and Sciences. November 10-14, Belo Horizonte, MG.

Fagundes Netto, J.R., Fabre, J., Péresson, L., 1999, "Shape of long bubbles in horizontal slug flow". International Journal of Multiphase Flow, Vol. 25, pp. 1129-1160.

Hirt, C.W., Nichols, B.D., 1981, "Volume of Fluid (VOF) Method for the Dynamics of Free Boundaries". Journal of Computational Physics 39(1), pp. 201-225.

Hutchinson, B. R. and Raithby, G.D., 1986, "A Multigrid Method Based on the Additive Correction Strategy". Numerical Heat Transfer, Vol. 9, pp. 511-537.

Leonard, B. P., 1979, "A stable and accurate convective modeling procedure based on quadratic upstream interpolation". Comput. Method Appl. Mech. Eng. Vol. 19, pp. 59–98.

Orell A., 2004, "Experimental Validation of a simple model gas-liquid slug flow in horizontal pipes". Chemical Engineering Science, Vol. 60 (2205), pp. 1371-1381.

Rosa, E. S., Fagundes Netto, J.r., 2004, "Viscosity Effect and Flow Development in Horizontal Slug Flows" 5th International Conference on Multiphase Flow, ICMF" 04 Yokohama, Japan, May 20-June 4, Paper No. 306.

Taitel, Y. & Barnea, D.. 1990, "Two–phase slug flow. Adv. Heat Transfer", Vol. 20, pp. 83–132.

Taitel, Y., Sarica, C., Brill, J.P., 2000, "Slug flow modeling for downward inclined pipe flow: theoretical considerations", International Journal of Multiphase Flow, Vol. 26, pp. 833–844.

Wallis, G.B., 1969. One-dimensional Two-phase Flow, McGraw-Hill, Inc, New York.

Yakhot, V., Orszag, S. A., Thangam, S., Gatski, T. B., Speziale, C. G., 1992. "Development of Turbulence Models for Shear Flows by a Double Expansion". Technique Phys. Fluids A. 4 (7), pp. 1510-1520.